PLOS ONE

RESEARCH ARTICLE

Cellular and biochemical response to chaperone versus substrate reduction therapies in neuropathic Gaucher disease

Margarita M. Ivanova‡*, Julia Dao, Neil Kasaci, Benjamin Adewale, Shaista Nazari, Lauren Noll☯, Jacqueline Fikry☯, Armaghan Hafez Sanati, Ozlem Goker-Alpan‡

Lysosomal and Rare Disorders Research and Treatment Center, Fairfax, VA, United States of America

☯ These authors contributed equally to this work.
‡ MMI and OGA also contributed equally to this work.
* mivanova@ldrtc.org

Citation: Ivanova MM, Dao J, Kasaci N, Adewale B, Nazari S, Noll L, et al. (2021) Cellular and biochemical response to chaperone versus substrate reduction therapies in neuropathic Gaucher disease. PLoS ONE 16(10): e0247211. https://doi.org/10.1371/journal.pone.0247211

Editor: Israel Silman, Weizmann Institute of Science, ISRAEL

Received: February 1, 2021

Accepted: October 12, 2021

Published: October 25, 2021

Data Availability Statement: All relevant data are within the manuscript and its Supporting Information files.

Funding: The authors received no specific funding for this work.

Competing interests: The authors have declared that no competing interests exist.

Abstract

Gaucher disease (GD) is caused by deficiency of the lysosomal membrane enzyme glucocerebrosidase (GCase) and the subsequent accumulation of its substrate, glucosylceramide (GC). Mostly missense mutations of the glucocerebrosidase gene (*GBA*) cause GCase misfolding and inhibition of proper lysosomal trafficking. The accumulated GC leads to lysosomal dysfunction and impairs the autophagy pathway. GD types 2 and 3 (GD2-3), or the neuronopathic forms, affect not only the Central Nervous System (CNS) but also have severe systemic involvement and progressive bone disease. Enzyme replacement therapy (ERT) successfully treats the hematologic manifestations; however, due to the lack of equal distribution of the recombinant enzyme in different organs, it has no direct impact on the nervous system and has minimal effect on bone involvement. Small molecules have the potential for better tissue distribution. Ambroxol (AMB) is a pharmacologic chaperone that partially recovers the mutated GCase activity and crosses the blood-brain barrier. Eliglustat (EGT) works by inhibiting UDP-glucosylceramide synthase, an enzyme that catalyzes GC biosynthesis, reducing GC influx load into the lysosome. Substrate reduction therapy (SRT) using EGT is associated with improvement in GD bone marrow burden score and bone mineral density parallel with the improvement in hematological parameters. We assessed the effects of EGT and AMB on GCase activity and autophagy-lysosomal pathway (ALP) in primary cell lines derived from patients with GD2-3 and compared to cell lines from healthy controls. We found that EGT, same as AMB, enhanced GCase activity in control cells and that an individualized response, that varied with *GBA* mutations, was observed in cells from patients with GD2-3. EGT and AMB enhanced the formation of lysosomal/late endosomal compartments and improved autophagy, independent of *GBA* mutations. Both AMB and EGT increased mitochondrial mass and density in GD2-3 fibroblasts, suggesting enhancement of mitochondrial function by activating the mitochondrial membrane potential. These results demonstrate that EGT and AMB, with different molecular mechanisms of action, enhance GCase activity and improve autophagy-lysosome dynamics and mitochondrial functions.

Introduction

Gaucher disease (GD) (OMIM 23080, 231000, 231005), the most common lysosomal storage disorder (LSD), is caused by pathologic *GBA* variants (OMIM 606463), resulting in the deficiency of the lysosomal membrane enzyme glucocerebrosidase (GCase) (EC 3.2.1.45). The *GBA* mutations lead to misfolding of GCase in the endoplasmic reticulum with the inhibition of proper trafficking and targeting to the lysosomes, and as a result, the deficient enzymatic activity and chronic accumulation of the substrate glucosylceramide (GC) in the lysosomes [1]. The major phenotypic presentations of GD are based on whether the CNS is impacted or not. GD type 1 is the non-neuropathic form, whereas types 2 and 3 (GD2 and GD3) are "neuropathic" GD. GD3 phenotypes are very heterogeneous; however, patients can present with horizontal ophthalmoplegia and varying neurological signs, such as progressive myoclonus, cerebellar ataxia, cognitive changes, or dementia in some cases [2]. The majority of *GBA* missense variants in patients with GD3 include L444P (L483P) (77%) and D409H (D448H) (7%) [3, 4]. Patients with L444P represent a phenotypically very diverse group with a range of systemic disease severity and neurological involvement [4]. The unique presentation with cardiac involvement, corneal clouding, and hydrocephalus is reported mainly in patients with homozygous D409H variants. In GD3, the disease onset is before 2 years of age, and with neurological symptoms in half of the cases. Psychomotor development is affected mostly. Seizures may occur later or manifest as myoclonic epilepsy resistant to antiepileptic drugs. Severe splenomegaly is almost always present and is associated with thrombocytopenia in 60% of cases. Growth retardation (30% of patients) may be the first sign, sometimes associated with cachexia. Lung lesions are sometimes observed, a result of pulmonary infiltration by Gaucher cells or sometimes due to recurrent aspiration [2]. GD type 2 (<5% GD cases) presents in infants aged 3–6 months old with early, severe, and rapidly progressive neurological involvement. Rigidity of the neck and trunk (opisthotonus), bulbar signs (particularly swallowing abnormalities), oculomotor paralysis, unilateral or bilateral alternating strabismus, followed by fixed strabismus are common presentations for the disease [2]. The mean survival age for GD2 without intervention is 11.7 months (range 2–25 months). Before the advent of ERT, children with GD3 succumbed to complications such as portal hypertension and bleeding of esophageal varices, with significantly reduced lifespans.

ERT is the standard of care in GD for the treatment of systemic symptoms, such as splenomegaly, hepatomegaly, thrombocytopenia, and low platelets [2, 5]. However, ERT is not effective in treating CNS pathology because of a lack of access through the Blood-Brain Barrier (BBB). Other alternative therapy modes to access CNS are using small molecules that may cross BBB, such as "new generation forms of SRT and pharmacologic chaperones (PCT) [6]. Glycosphingolipids (GSLs) are involved in a large number of cellular processes, including signal transduction, membrane trafficking, and the formation of cytoskeletal domains. GC is the primary precursor of complex glycosphingolipids, and its synthesis and degradation are crucial steps for GSL metabolism. GC is formed by UDP-glucosylceramide synthase (UGCG) in the Golgi apparatus from its precursor ceramide (Fig 1). As an inhibitor of the cytoplasmic enzyme UGCG, EGT is prescribed for type 1 GD patients [7, 8]. In clinical trials, EGT has demonstrated significant efficacy for improving systemic disease manifestations, including hepatosplenomegaly, hematologic manifestations, and bone involvement in subjects with GD type 1 [7, 9]. However, EGT is not effective for treating GD's neuropathic forms due to the lack of ability to cross the BBB [3]. A new generation of UGCG inhibitor, venglustat (GZ/SAR402671), could cross the BBB and is in trials for Gaucher, Fabry, and Tay-Sachs diseases [3]. GD and GD-Parkinson mouse studies and cell models currently provide evidence that the related compound (GZ667161) reduces GC's level in the brain [10].

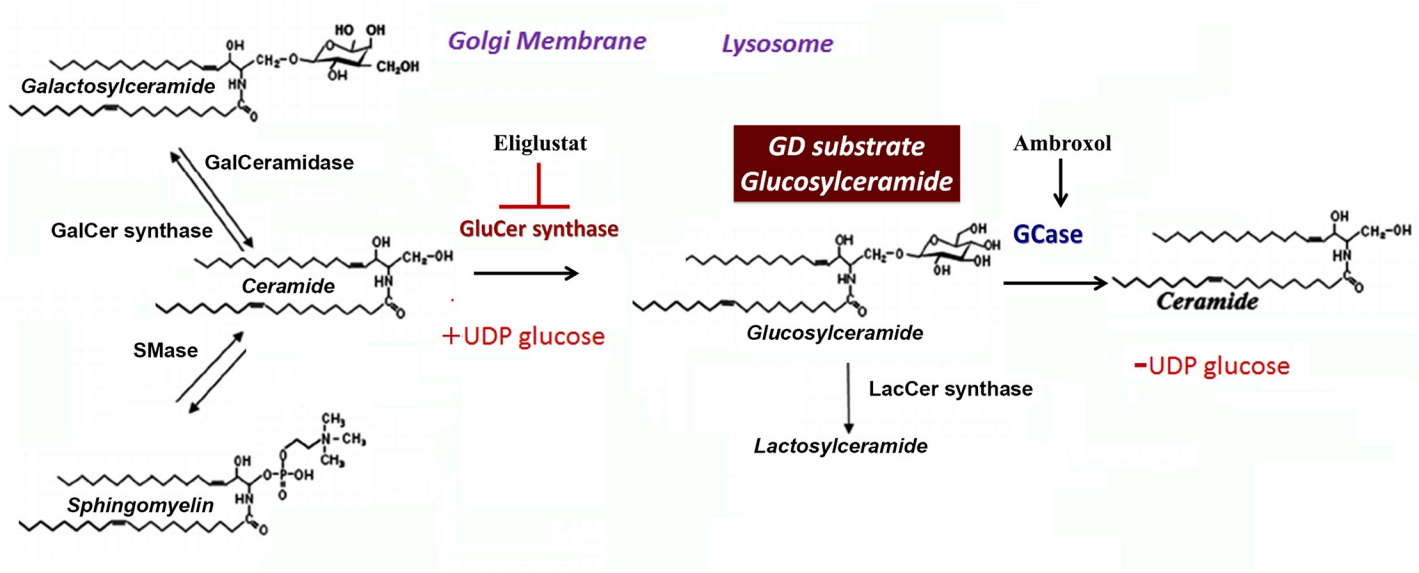

Fig 1. Glucosylceramide (GC) metabolism in Gaucher diseases. Ceramide, glucosylceramide shift between the Golgi apparatus and lysosomes. Ceramides, generated in the ER, are transported to the Golgi apparatus, where UDP-glucosylceramide synthase (UGCG synthase) converts Cer to GC on the cytosolic side of the Golgi [19]. After, GC transport back into the ER. To transport ceramide to lysosome, GS, GCase, and saposin C (reaction facilitator) are embedded within intralysosomal membrane where cleavage of lipid tail will occur [20]. Eliglustat inhibits UGCG synthase. Ambroxol increases GCase enzyme activity.

https://doi.org/10.1371/journal.pone.0247211.g001

Other therapy alternatives for GD using small molecules are enzyme-enhancement (EET) or pharmacologic chaperone (PCT) therapies. PCT is based on the small molecules' ability to fold the misfolded mutant enzyme, deliver an enzyme to the lysosomes, and increase enzymatic activity [6]. The advantage of PCT is that the small molecules can cross the BBB and could potentially treat the neurological symptoms. An open-label pilot study with ambroxol (AMB) showed promising results in neuronopathic GD patients with N188S, G193W, F213I/RecNciI, and D409H/IVS10^{-1}G>A genotypes [11–13]. AMB demonstrated good tolerability while enhancing GCase activity and improving neurological manifestations [14]. AMB interacts with active and non-active sites of enzymes, explaining the mixed type of activation/inhibition and pH-dependent activity [11, 15, 16]. Ambroxol stabilizes GCase, and demonstrates inhibitory GCase activity at neutral pH and absence of inhibitory effect at the acidic pH of lysosomes [11]. Different G*BA* mutations have different effects on protein folding, trafficking, and enzymatic activity, and AMB demonstrates a mutation-dependent chaperoning profile [11, 15, 17]. The *in vitro* response to AMB is rather "personalized" and differs even for siblings [11]. In primary cell lines from patients with N370S/L444P, AMB shows a positive effect; however, in cells derived from patients with L444P/L444P, there is no uniform GCase activation after AMB treatment [11, 15, 18]. In the present study, we investigate *in vitro* effects of EGT and AMB on GCase enzymatic activity, the autophagy-lysosomal pathway, and mitochondrial activity.

Materials and methods

Patients

The patient's demographics and clinical characteristics are presented in **Table 1**. The diagnosis of GD was confirmed by enzymatic activity and molecular analysis. As expected, among the pathogenic variants, L444P (L483P) variant was highly prevalent in both homozygous (12/15) and compound heterozygous states (3/15), including the recombinant alleles. Overall, eight

Table 1. Demographics, clinical and molecular characteristics of subjects with GD.

#	Gender	Age	Ethnicity	*GBA* genotype	GD Type	Gcase residual activity
1	M	15	Caucasian	L444P/L444P	GD3	4.2%
2	M	8	Caucasian	L444P/L444P	GD3	3.8%
3	F	1	Caucasian	L444P/L444P; A456P	GD3	0.8%
4	M	8	Asian	L444P/L444P	GD3	3.5%
5	F	8	Caucasian	L444P/L444P	GD3	4.8%
6	M	1	Caucasian	L444P/L444P; RecΔ55, Rec NciI	GD2	0.66%
7	M	2	Caucasian	L444P/L444P; R495P/R495P; A456P	GD2	2.5%
8	F	4	Hispanic	L444P/L444P D409H/A456P	GD2	2.7%
9	M	<1	African American	L444P/D409H	GD2-3	2%
10*	F	40	Caucasian	L444P/R463C	GD3	4.7%
11*	M	22	Other	L444P/L444P	GD3	10.4%
12*	F	22	Hispanic	L444P/L444P	GD3	9.2%
13*	M	21	Hispanic	L444P/L444P	GD3	9.4%
14*	F	12	Hispanic	L444P/L444P	GD3	8.7%
15#	M	<1	Caucasian	GBA-GBAp recombination intron1, L444P	GD2	<1%

*: PBMC only

Fig 3B and 3C.

Patogenic GBA variants:

L444P (c.1448T>G (p.Leu483Arg); protein change variants: L483P, L396P, L434P, L444P); RecΔ55 (c.1265_1319del); Rec NciI (c.14448C-1498C); D409H (c.1342G>C (p.Asp448His); protein change variants: D448H, D361H, D3999H, D409H); R463C (c.1504C>T (p.Arg502Cys), protein change variants: R502C, R415C, R453C R463C).

https://doi.org/10.1371/journal.pone.0247211.t001

patients have missense L444P/L444P mutation, and among patients who have multiple complex alleles, the L444P (L483P) variant was present in all seven of them. The clinical protocol was approved by the ethics committees and data protection agencies at all participating sites (Western Institutional Review Board, WIRB # 20131424). Written informed consent or assent was obtained from patients or parents/guardians to collect samples and analyze the data.

Materials

Eliglustat hemitartrate (EGT) (MCE, MedChem Express, NJ, USA), ambroxol hydrochloride (AMB) (Abcam, Cambridge, UK). Human anti-glucocerebrosidase (GBA) antibodies (Gen-Tex), LAMP1, and LC3A/B antibodies (Cell signaling technology, Danvers, MA, USA). NuPAGE SDS running buffer, bolt 8% Bis-Tris Plus gel, Novex ECL chemiluminescent substrate reagents, sample reducing agents, media 106, low serum growth supplement kit, BCA protein assay kit (Thermo Fisher Scientific, Rockford, IL, USA). Sodium taurocholate hydrate, 4-Methylumbelliferyl β-D-glucopyranoside (Sigma-Aldrich, St. Louis, MO, USA), normocin (InvivoGen, San Diego, CA, USA).

Isolation and preparation of primary skin fibroblasts

Skin biopsies from GD patients were collected following standard procedures and an aseptic technique, from the inner aspect of the upper arm in adults and older children or upper leg in infants. Fibroblast cells were grown in complete M106 media (Life Technologies, Grand Island, NY, USA) as previously described [15]. The primary fibroblasts after passage 5–6 were grown and treated in Dulbecco's modified Eagle's media (DMEM) with 10% fetal bovine serum (FBS). Cultures were terminated before passage 10.

Isolation and purification of peripheral blood monocytes (PBMC)

PBMC were purified from blood samples from GD patients using Lymphoprep™ reagent and SepMate™ tubes (Stemcell Technologies, Vancouver, Canada). Lymphoprep™ was added to the lower compartment of the SepMate tube. Blood was mixed with PBS containing 2% fetal bovine serum (FBS) in a 1:1 ratio and then layered on top of Lymphoprep™ following the manufacturer's protocol. PBMC cells were cultured in RPMI 1640 media with 5% FBS.

Differentiation of macrophages from PBMC

Freshly isolated PBMC are used for macrophage differentiation following the procedure described below [15]. RPMI 1640 medium with 10% FBS was used to isolate, resuspend, and culture PBMCs. For macrophage differentiation, the media RPMI 1640 was supplemented with 10% FBS, 1% normocin, 2mM glutamine, 1% Na-pyruvate, 1% non-essential amino acids (NEEA), and 50 ng/ml human recombinant M-CSF (ThermoFisher Scientific, Rockford, IL, USA). After six days of PBMC culture, 100% by volume of fresh complete macrophage differentiation media was added, and two days later, the media was replaced. On day ten, macrophages were treated with AMB and EGT at indicated time intervals and concentrations. In GD, it is suggested that the macrophages have an activated status; in this study, some PBMC differentiated into macrophages spontaneously. In these experiments, PBMC were collected for analysis after treatment, and naturally differentiated macrophages were stained with DAL-Green, LysoTracker Red, or MitoTracker Red CMXRos for further evaluation.

Protein isolation and western blot analysis

Whole-cell extracts (WCE) were prepared in radioimmunoprecipitation (RIPA) buffer. Protein concentrations were determined using the BCA protein assay kit (ThermoFisher Scientific, Rockford, IL, USA). 30 μg of WCE were separated on mini protein TGX stain-free gel and electroblotted using the PVDF transfer membrane (Bio-Rad, Hercules, CA, USA). The ChemiDoc^{TM} MP imaging system (Bio-Rad, Hercules, CA, USA) was used to visualize and quantitate optical density (IOD) for each band. The IODs of bands of interest were normalized to the loading control, beta-actin, and the normalized value of the controls were set to 1 for comparison between separate experiments.

Measurement of GCase activity

GCase enzymatic activity in cells was carried out using 4-methylumbelliferyl b-D-glucopyranoside. Released 4-methylumbelliferone was measured using a fluorescence plate reader (excitation 360 nm and emission 460 nm) [21, 22]. The reaction was started by the addition of 5 or 10 μg of protein into substrates solution in 0.1 M citrated buffer, pH 5.2, supplemented with sodium taurocholate (0.8% w/v). The reaction was terminated by adding 0.4 ml of 0.2 M glycine sodium hydroxide buffer (pH 10.7).

Measurement of lysosome levels

The LysoTracker Red assay was used to follow the manufacturer's protocol (LifeTechnology, ThermoFisher, Rockford, IL, USA). LysoTracker Red (50 nM) was added to live cells in the presence of AMB and EGT treatments and stained 30 min. Then, cells were stained with Hoechst and washed 3 times with PBS before analysis. The red fluorescence of LysoTracker was measured in triplicates using a SpectraMax M2 microplate reader with an excitation wavelength: 577 mm; emission wavelength: 590 nm (Molecular Devices, Sunnyvale, CA, USA).

Data was normalized to untreated cells. The resulting fluorescence was visualized by fluorescent microscopy (Evos, Hatfield, PA, USA).

Mitochondrial mass staining

According to the manufacture protocol, the MitoTracker Red CMXRos mitochondrial kit (ThermoFisher Scientific) was used to quantify mitochondrial activity by measuring the membrane potential. Nuclear Hoechst dye was used as an index of cell contents. Cells were stained with a fluorescence probe for 30 min and then washed with PBS. MitoTracker Red CMXRos signal was measured in triplicates using SpectraMax M2 microplate reader with excitation/emission 577–590, or the fluorescence signal was visualized by fluorescent microscopy (Evos, Hatfield, PA, USA).

Mitochondrial membrane potential assay

The mitochondrial membrane potential was determined using the JC-1 Mito-ID membrane Potential Kit (Dojindo Molecular Technologies, Inc). In the energized inner membrane, the mitochondria produced an orange fluorescence signal. If cells exhibit a shift from orange to green fluorescence: mitochondrial function becomes compromised. After five days of treatment with AMB and EGT, fibroblasts were stained with mito-ID membrane potential dye solution in clear-bottom black 96-well tissue culture plates for 30 min. After incubation, cells were washed three times with PBS, and the fluorescence signals were visualized by fluorescent microscopy (Evos Digital microscope, Evos, Hatfield, PA, USA). Flow cytometry for JC-1 in PBMC was perfomed using a BD Accuri C6 flow cytometer (BD Bioscience, San Jose, CA, USA) according to Accuri cytometer protocol for JC-1 assay.

Mitochondrial computational analysis

2D image-based mitochondrial analysis and network characteristics were performed using ImageJ. For network connectivity analysis, the "Skeleton 2D/3D" command was used to calculate the number of branches and branch junctions in the skeletonized network [23]. The analysis tags pixel/voxels in a skeleton image and counts junctions, triple and quadruple points, and branches, and the program measured junction voxels and endpoints. The voxels are classified as endpoint voxels (if they have less than two neighbors) and junction voxels (more than two neighbors). The endpoint voxels are displayed in blue and junction voxels are displayed in purple. Briefly, fluorescence images of live cells were captured using 40x magnification with large format 2048 X 2048 pixel with the same time exposure and brightness. Selected groups of 2–4 cells were first cropped from the original image to allow analysis on a cell-to-cell basis. The initial contrast of microscope images was enhanced, and residual background pixels were removed following program algorithm recommendation. The parameters of contrast and background were the same for all images.

Autophagy staining

DALGreen (Dojindo Molecular Technologies, Inc) was used for the detection of phagosome-lysosome fusion. In several experiments, DALGreen was co-stained with a lysosomal marker, LysoTracker Red. After DALGreen was stained, cells were washed with PBS three times and stained with Hoechst 33342 dye as an index of the nucleus. The resulting fluorescence was visualized by fluorescent microscopy (Evos, Hatfield, PA, USA).

Glucocerebrosidase and LAMP1 immunofluorescence staining

Cells were grown on coverslips and were incubated with 10 μM of AMB and 10 μM of EGT for five days. Cells were then fixed with cold methanol for 5 minutes and washed three times with cold PBS. After blocking with 3% BSA and 0.3% Triton X-100 in PBS for 1 h, primary antibodies GBA (β-glucosidase (A-16, sc-100544, Santa Cruz Biotechnology, Inc, CA, USA) and LAMP1 (D401S, Cell Signalling Technology, MA, USA) were added at a 1:500 dilution for ON $+4C^0$. The cells were stained with secondary antibodies labeled with Alexa-Fluor 488 and Alexa-Fluor 555 (ThermoFisher Scientific, Rockford, IL, USA). Cells were incubated with nuclear-DAPI staining. Images were obtained using the Evos^R Digital microscope (Evos, Hatfield, PA, USA).

Cell viability and cytotoxicity assay

Cell viability was evaluated colorimetrically by measuring the dehydrogenase activity with NADH released in the media using cell counting kit-8 (CCK-8, Dojindo Molecular Technologies, Rockville, MD, USA) according to the manufacturer's instruction. In brief, cells were seeded on 96-well plates at a density of 50% confluence. Then, the cells were treated with an increasing concentration of AMB and EGT or vehicle control (0.1% DMSO) for 24, 48, 72 h, and 5 days. CCK-8 was added, and absorbance (OD) at 450 nm was detected using the microplate reader (Molecular Devices, Sunnyvale, CA, USA). The IODs were normalized to the untreated control, and the normalized value of the controls was set to 100%.

ATP assay

The cell titer-Glo luminescent assay was used to measure the ATP levels (Promega, Madison, WI, USA). The fibroblasts were plated in 96-well white plates with clear bottoms. After AMB and EGT treatments, plates were divided, the half plate was used for CCK-8 assay, and the other half of the plate was used to measure ATP. 100 μl of CellTiter-Glo reagent was added directly to the samples, and after 15 min incubation, cells were analyzed by measuring bioluminescence signal in a Genini microplate reader (Molecular Device, San Jose, CA). Samples were run in triplicates.

LDH release assay

To assess the potential cytotoxicity of the AMB and EGT, the lactate dehydrogenase (LDH) release assay was performed. Control and GD3 fibroblasts were treated with increased concentration of AMB and EGT for 5 days, and supernatants were collected to a new white opaque 96-well plate. After adding the LDH reaction solution (LDH-Glo^{TM} Cytotoxicity Assay, Promega, Madison, WI), the plate was incubated for 30 min. The luminescence signal was read using a Gemini microplate reader (Molecular Device, San Jose, CA).

Immunofluorescence microscopy analysis

Interactive analysis ImageJ plugins (NIH, Bethesda, MD, USA) with the option of "Color Inspector 3D" were used to analyze the colocalization projection of GBA and LAMP1. Pixels with red intensity values (GBA) lay on the R (red) axis, and pixels with green intensity values (LAMP1) lay on the G (green) axis. The areas of colocalization GBA and LAMP1 are seen in yellow. Pixels with blue intensity values (nucleus) lay on the B (blue) axis. The 3D plot reveals colocalized red and green pixels are located along the diagonal (yellow color), while those with no colocalization occupy left (GBA) or right (LAMP1) portions.

Statistical analysis

Statistical analyses were performed using Student's *t*-test with 2-tailed distribution and 2-sample equal variance or 1-way ANOVA followed by Student-Newman-Keuls using GraphPad Prism (GraphPad, San Diego, CA, USA).

Results

EGT, similar to AMB, induces GCase activity

As a GCase chaperone, AMB was demonstrated to increase GCase in cells with N370S/N370S or L444P/N370S *GBA* mutations. However, in cell lines from GD2 or G3 patients with L444P/L444P or L444P in combination with other *GBA* variants, the GCase activity was not uniformly enhanced [11, 15, 24]. The effect of EGT on GCase activity was never thoroughly investigated. Thus, EGT and AMB's effect on GCase enzyme activity was compared to primary fibroblasts derived from GD2 and GD3 patients with different *GBA* mutations (Table 1). Control or GD2-3 fibroblast lines were treated with increasing concentrations of AMB and EGT for 5 days, and enzyme activity was measured. EGT increased GCase activity in control fibroblasts in a concentration-dependent manner, similar to AMB (Fig 2A).

In cells derived from patients with L444P/L444P, there was no uniform GCase activation after AMB and EGT treatments (Fig 2A). AMB increased GCase activity in P1 and P2 fibroblasts, and EGT increased GCase activity in P1 fibroblast in a concentration-dependent manner (Fig 2A). P3 fibroblasts increased GCase activity in the presence of 100 μM of AMB only. In P2 fibroblasts, GCase activity increased in the presence of 10 μM of EGT, and in P5, there was increased enzymatic activity in the presence of 1 μM of EGT. AMB and EGT did not affect GCase activity in P4 fibroblasts (Fig 2A). Overall, in 3 out of 5 cell lines, there was an elevation of GCase activity in the presence of AMB and EGT (Fig 2A).

GD2 fibroblasts demonstrated a "personalized" response to AMB and EGT treatments (Fig 2B). In P6 and P9 fibroblasts with L444P/L444P; RecΔ55, Rec NciI, and L444P/D409H *GBA* variations, there was increased enzymatic activity in the presence of AMB and EGT in a concentration-dependent manner (Fig 2B). In P7 fibroblasts (L444P/L444P; R495P/R495P; A456P), GCase activity increased in the presence of 10 μM of AMB and 1 μM of EGT. Only 1 μM of EGT increased GCase in P8 fibroblasts with L444P/L444P; D409H; A456P *GBA* variations (Fig 2B). In absolute terms, the individual levels of GCase in AMB and EGT treated GC cells were still low compared with controls (Fig 2C).

PBMC was collected from five GD3 patients to examine if EGT induced GCase in PBMCs and macrophages (S1 Fig). EGT, as well as AMB, increased GCase activity in controls and GD3 PBMC and macrophages except for P13 GD3 cells (S1A and S1B Fig).

Both EGT and AMB improve lysosomal functions

AMB accelerates the folding and trafficking of GCase to lysosomes and restores lysosomal functions [15, 24, 25]. To investigate if EGT mediates the trafficking of GCase to lysosomes, control fibroblasts were treated with both compounds. Staining with anti-GBA (red) and anti-LAMP1 (green) antibodies confirmed that EGT and AMB induce lysosomal localization of GCase in WT and GD2 fibroblasts (Fig 3A and 3B). Color Inspector 3D analysis showed full co-localization GBA with the lysosomes in the presence of AMB and increasing GBA-LAMP1 co-localization after EGT treatment in GD2 fibroblasts (Fig 3C). Then, to investigate lysosomal biogenesis, we compared the effects of EGT and AMB on LAMP1 levels. Western blots showed a significant increase in LAMP1levels in fibroblasts derived from patients with L444P/L444P or L444P/L444P;D409H;A456P *GBA* mutations in response to AMB and EGT treatments.

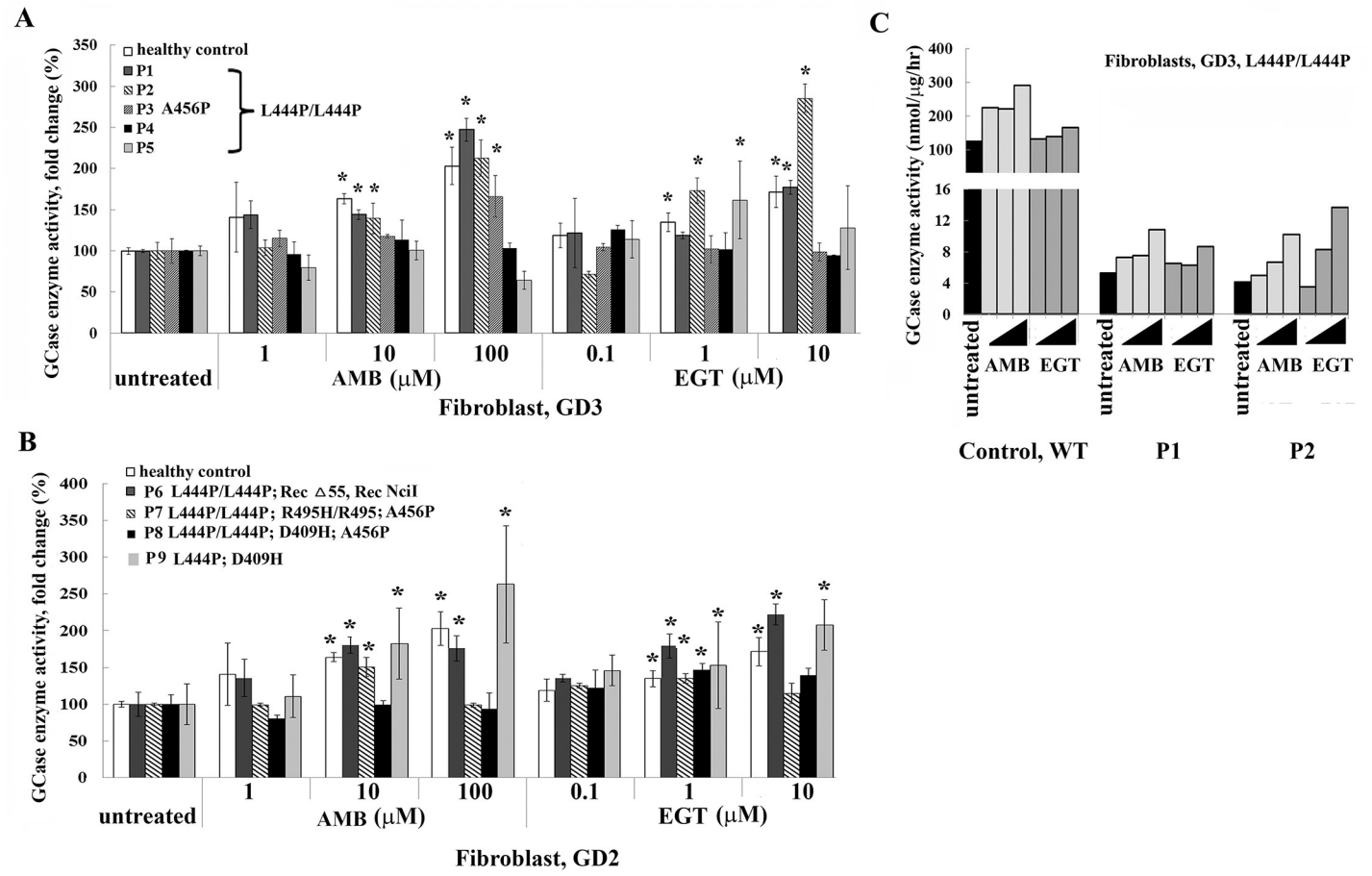

Fig 2. Assessing GCase activity in primary fibroblasts treated with AMB and EGT. A. Fibroblasts derived from healthy controls and GD3 patients with the genotypes L444P/L444P and L444P/L444P/A456P were cultured for 5 days in the presence of increasing concentrations of AMB or EGT. Relative GCase enzyme activity was estimated as a percentage towards untreated control. Each bar represents the average +/- STDEV. * $p<0.05$ compared with an untreated group. **B.** Fibroblasts derived from GD2 with different *GBA* mutations, as indicated, were treated for 5 days in the presence of AMB and EGT. Relative GCase enzyme activity was estimated as a percentage towards untreated control. Each bar represents the average +/- STDEV. * $p<0.05$ compared with an untreated group. **C.** Comparing GCase enzyme activity estimated as nmol/μg/hr in healthy control fibroblasts and GD3 fibroblasts.

https://doi.org/10.1371/journal.pone.0247211.g002

Furthermore, AMB but not EGT increased LAMP1 levels in a concentration-dependent fashion (Fig 3D).

The LysoTracker Red, an acid-dependent dye, has been used for labeling lysosomal/late endosomal compartments in live cells. Fibroblasts and PBMC were treated with EGT and AMB for five days. Upon treatment with 10, 100 μM of AMB and 1, 10 μM of EGT, the number of acidic vesicles increased in control, GD2, and GD3 fibroblasts (Fig 4). Furthermore, an increase in the LysoTracker Red intensity also was observed in control and GD3 PBMC in the presence of EGT and AMB (S2 Fig). Altogether, the data suggests that activation of lysosomal function is a universal response to EGT and AMB treatments.

EGT and AMB improve autophagy dynamics independent of GCase activation

The accumulation of GC in the lysosomes is suggested to impair lysosomal functions and inhibit autophagic flux [26, 27]. Autophagy and lysosomal staining with DALGreen and LysoTracker Red is used to compare EGT and AMB effects on autophagy-lysosomal function.

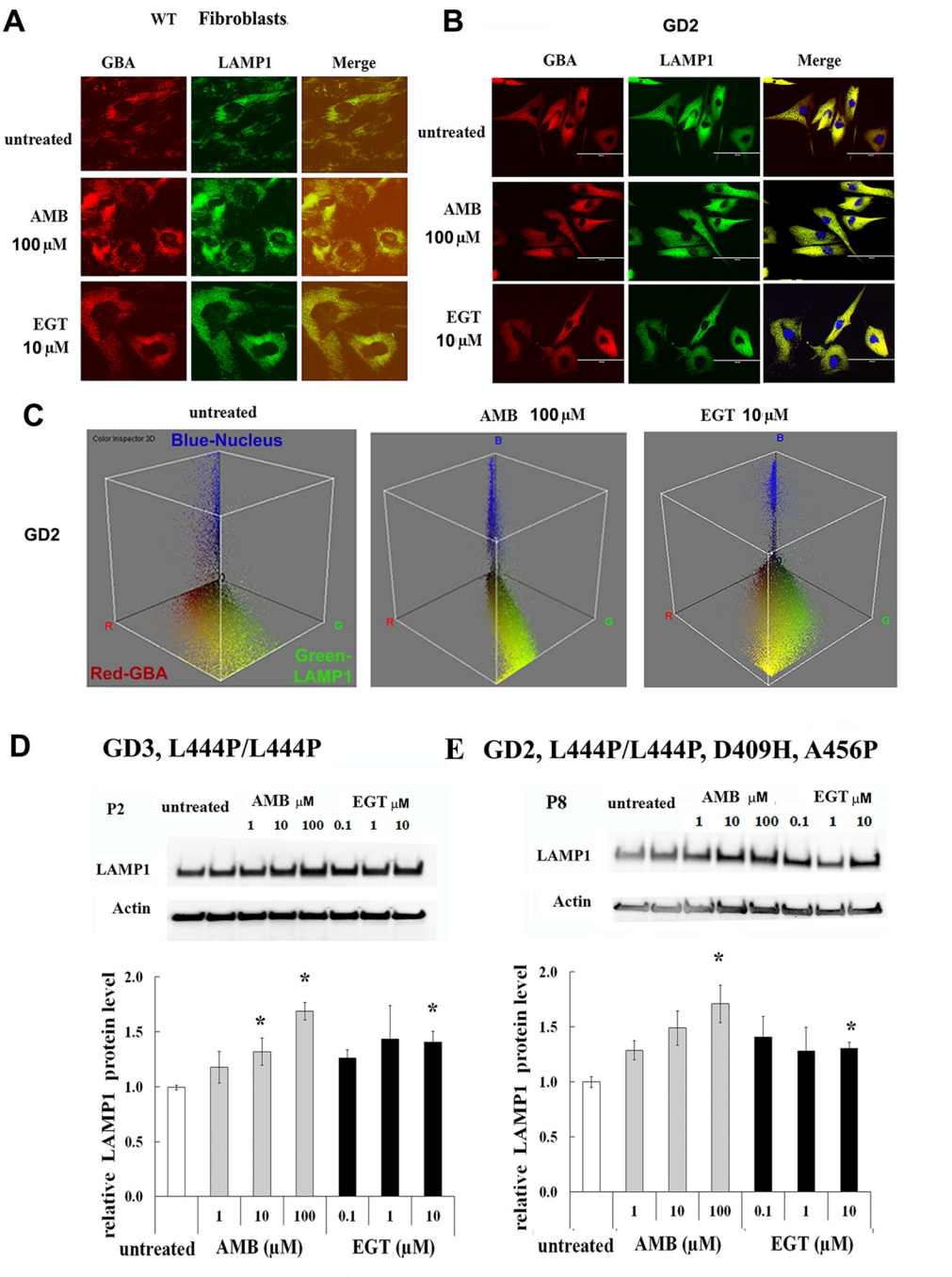

Fig 3. AMB and EGT induce lysosomal trafficking and LAMP-1 level in primary fibroblasts. A-B. Fluorescence microscopy images of control fibroblast (A) and GD2 fibroblast (B). The cells were treated with 10 μM AMB and 10 μM EGT for five days. Each set of three side-by-side images shows anti-GBA (red), anti-LAMP1 (green color) antibodies, and merged images. The yellow color indicates colocalization of GBA and LAMP1 in the lysosome. **(C)** The interactive 3D color inspector plots displayed a three-dimensional graph of pixel distribution of images of GD2 fibroblasts. Nucleus (blue), GBA (red) and LAMP1 (green) colocalization. **D.** Top row represents the western blot of LAMP1 in fibroblasts derived from GD3 patients. Actin is used as the loading control. P1, P2, P4, and P5 (n = 4). * $p<0.05$ compared with an untreated group. **E**. The top: western blot of LAMP1 in GD2 fibroblasts derived from patient 8 with L444P/L444P;D409H;A456P genotype. The bottom: quantification of the relative level of LAMP1/actin from P8. Each bar represents the average +/- STDEV from three independent experiments. * $p<0.05$ compared with an untreated group.

https://doi.org/10.1371/journal.pone.0247211.g003

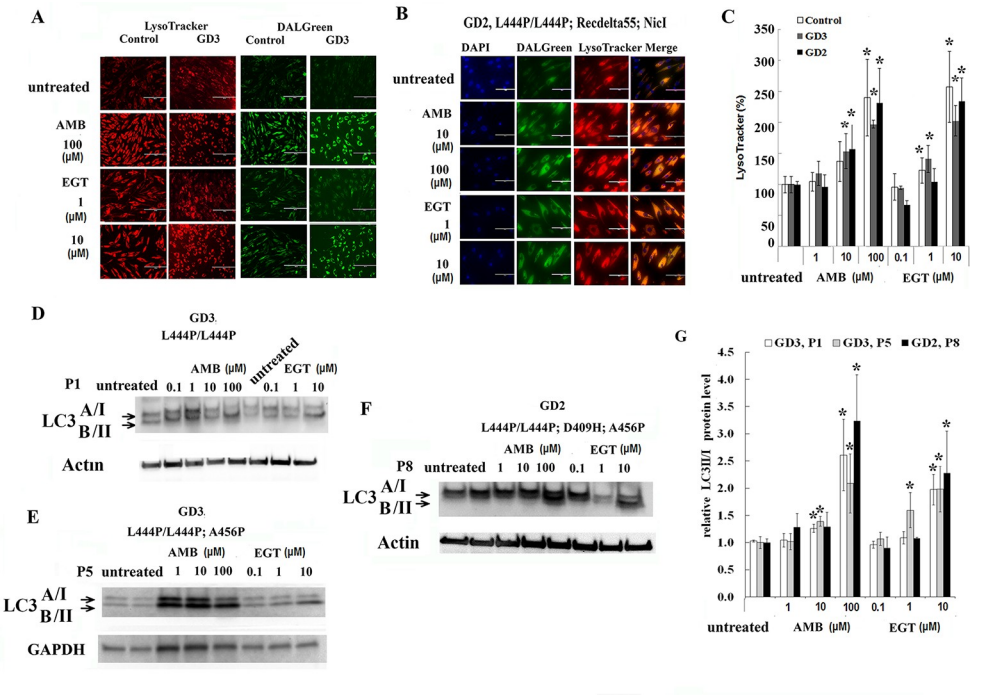

Fig 4. EGT and AMB improve autophagy and lysosomal dynamics. A. The lysosome (red) and autophagy (green) fluorescent staining in live control and GD3 (P5) fibroblasts with L444P/L444P *GBA* mutation after AMB and EGT treatments for five days. **B.** Lysosome and autophagy colocalization analysis in GD2 fibroblasts after treatment with AMB and EGT for five days. **C.** Quantification of fluorescence intensity of lysosomes. The signal intensity in untreated cells was set at 100%. The graph indicates the relative intensity value of fluorescence signal related to LysoTracker in control fibroblasts, GD3 fibroblasts with L444P/L444P, and GD2 fibroblasts. Values are expressed as average ± STDEV. **D, E, and F.** Following AMB and EGT treatments, representative western blots showing LC3-I/LC3-II protein expression level in GD3 fibroblast derived from patients: P1 (D), P5 (E), and GD2 patient P8 (F). **G.** Quantification of the relative level of LC3-II to LC3-I. Each bar represents the average +/- SEM. * $p<0.05$ compared with an untreated group. Student T-test, 2 tail, 2 type.

https://doi.org/10.1371/journal.pone.0247211.g004

DALGreen autophagy detection kit is selective for monitoring late-phase autophagy and autolysosomes [28]. The rate of autolysosome staining in control, GD3 and GD2 fibroblasts were increased after treatment with 1, 10 μM of EGT and 10, 100 μM of AMB (Fig 4A and 4B). Merged images confirm the autophagosomes' activation and fusion with lysosomes in GD2 fibroblasts (Fig 4B). Similar to fibroblasts, the autolysosomes staining in PBMC was significantly increased in control and GD3 cells after five days of treatment with 10 μM of EGT and 100 μM of AMB (S2 Fig). Merged analysis of autophagosomes with LysoTracker confirmed autophagosome activation and fusion with lysosomes (S2 Fig). Autophagy flux marker LC3I-II analysis showed a significantly increased level of LC3-II in GD3 fibroblasts and GD2 fibroblasts with L444P/L444P; D409H; A456P *GBA* mutations after EGT and AMB treatments in a concentration-dependent manner (Fig 4D–4G). Interestingly, AMB increased autophagy/lysosomal function in P5 fibroblasts without enhancing GCase activity (Fig 4E and 4G). In summary, AMB and EGT improved autophagy-lysosomal dynamics in primary cells derived from GD2 and GD3 patients.

EGT and AMB inhibit cell proliferation

To evaluate cytotoxic effects of EGT and AMB, control and GD fibroblasts were treated in the presence of various concentrations of EGT and AMB, and then the cell proliferation and

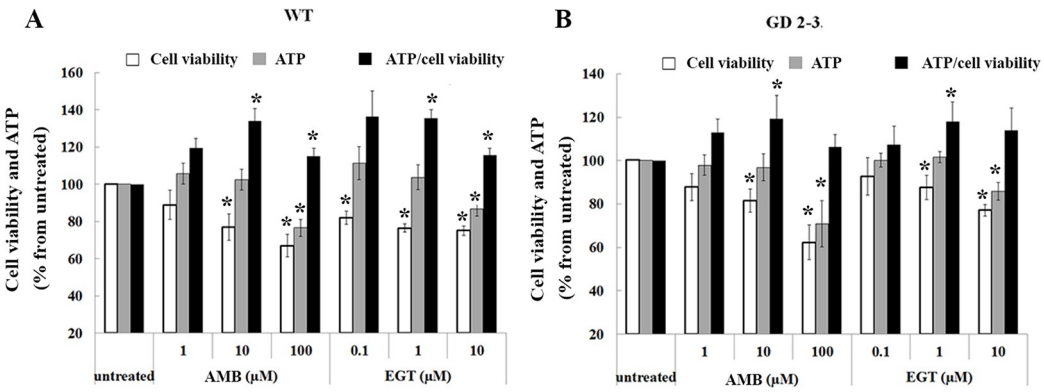

Fig 5. Assessment of cell viability and metabolic status in fibroblasts. A. Control (WT) fibroblasts were treated with 1, 10 or 100 μM of AMB and 0.1, 1 or 10 μM of EGT for 5 days and were submitted to the CCK-8 cell viability assay and ATP content. The obtain cell counting assay, CCK-8, and ATP results were normalized to the untreated cells. Additionally, the ratio ATP/CCK-8 (cell viability) was estimated. Values are expressed as average ±SEM, n = 3. * $p<0.05$ compared with an untreated group. **B.** Fibroblasts derived from three GD2 patients, P6 with L444P/L444P;RecΔ55;RecNCiI, P7 with L444P/L444P;R495P/R495P;A456P *GBA* variations, P9 with L444P/D409H, and one GD3 patient with L444P/L444P mutation, (P5) were treated with 1, 10, 100 μM of AMB and 0.1, 1,10 μM of EGT for 5 days. The CCK-8 cell viability assay and ATP content were analyzed. The obtained cell counting assay, CCK-8, and ATP results were normalized in relationship to the untreated cells. ATP/CCK-8 (cell viability) ratio was estimated. Values are expressed as average ±SEM, n = 4. * $p<0.05$ compared with an untreated group.

https://doi.org/10.1371/journal.pone.0247211.g005

viability assays were done. The number of viable cells was significantly decreased in control and GD2-3 fibroblasts in a concentration-dependent manner in the presence of both AMB and EGT (Fig 5A and 5B). Analysis of individual cell lines confirmed that the highest concentration of AMB and EGT decreased cell viability in GD fibroblasts derived from patients P5, P6, P7, and P9 (S3 Fig). Moreover, time course treatment verified that the highest concentration of AMB and EGT decreased the number of cells after 24 h treatment (S4 Fig), possibly due to cell proliferation inhibition. Then, we tested the response control, GD2, and GD3 fibroblasts to AMB and EGT exposure by measuring the intracellular ATP level. ATP levels significantly decreased in all cell lines in a dose-dependent manner (Fig 5 and S3 Fig). The ATP/cell viability ratio was analyzed to assess the reason for ATP inhibition: either due to reducing the number of cells or alteration of mitochondrial function. The ATP/cell viability ratio was increased in control fibroblasts after treatment with 10, 100 μM of AMB, and 1, 10 μM of EGT (Fig 5A). In GD 2–3 cells, 10 μM of AMB and 1 μM of EGT increased ATP/cell viability ratio (Fig 5B). Analysis of individual GD cell lines verified elevation of ATP/cell viability ratio in AMB and EGT treated fibroblasts: P5, P6, and P9 (S3 Fig). AMB, not EGT, displayed the elevation of ATP/cell viability ratio in GD2 fibroblasts derived from patient 7 (S3D Fig). The release of the LDH enzyme in media suggests the loss of membrane integrity, the active form of apoptosis or necrosis. The cytotoxic effect of AMB and EGT on control and GD3 fibroblasts, which were treated for five days, were analyzed by LDH assay. The results demonstrated no increase in the level of LDH release in treated cells (S5 Fig). In summary, CCK-8, ATP, and LDH results suggest that EGT and AMB inhibit cell proliferation and trigger mitochondrial energy metabolism in healthy control and GD2-3 cells.

EGT and AMB enhance mitochondrial metabolism

Because both EGT and AMB increased ATP levels in fibroblasts, mitochondrial function was further assessed. To visually detect mitochondrial activity in live cells, we used a cell-permeable fluorescent dye, MitoTracker Red. The visual representation of mitochondrial mass and

quantitative analysis demonstrated a significant increase in mitochondrial activity in control (Fig 6A and 6B) and GD2-3 fibroblasts (Fig 6C and 6D) after both treatments in a concentration-dependent manner. Fig 6E description. We then analyzed the mitochondrial density using the skeleton algorithm [29, 30]. As shown in Fig 7, the analysis of the 2D images revealed a significant difference in mitochondrial density between untreated and AMB/EGT treated cells. Consistent with increased mitochondrial density, the number of junction voxels and end-point voxels were also increased in cells in the presence of AMB and EGT (Fig 7B).

The mitochondrial membrane potential (Δm) is generated by proton pumps (Complexes I, III, and IV), and is an essential component of the ATP process during oxidative phosphorylation. Normally, the levels of ATP and ΔΨm in the cell are kept stable. However, a decrease or rise of ΔΨm may induce apoptosis, which can be observed in various disease entities [31]. Therefore, we measured Δm using JC-1 dye in GD3 fibroblast and PBMC after treatment with 1, 10, 100 μM of AMB and 0.1, 1 and 10 μM of EGT for 5 days (Fig 8A and 8B). Healthy mitochondria have high Δm uptake dye and emit red fluorescence at 590 nm, damaged mitochondria with low Δm emit green fluorescence. JC-1 assay showed that AMB and EGT treatments increased red fluorescence intensity compared with untreated groups indicating activation of hyperpolarization of mitochondria (Fig 8A and 8B, S6A Fig). Flow cytometry analysis confirmed that untreated PBMC stained with JC-1 represented two distinct populations of cells with high JC-1 aggregates (with two subpopulations: intermediate ΔΨ P1 and high ΔΨ P2) and low JC-1 aggregates (low ΔΨ P3 and intermediate ΔΨ P4 subpopulations) (S6 Fig). Following

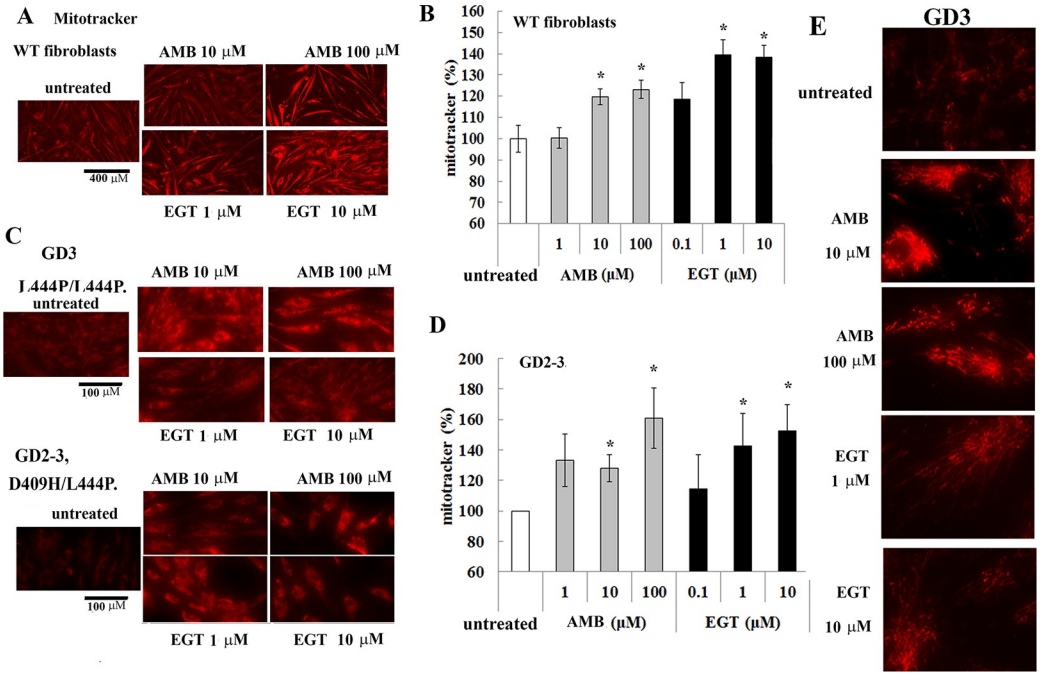

Fig 6. MitoTracker deep red staining in AMB and EGT treated fibroblasts. **(A)** The mitochondrial visualization in live control (WT) fibroblasts with AMB and EGT treatment for five days. Scale bar represents 400 μm. **(B)** Quantification of fluorescent intensities of mitochondria. The signal intensity in untreated cells was set at 100%. The graph indicates the relative intensity value of the fluorescence signal related to MitoTracker Red in control fibroblasts. Values are expressed as average ±STDEV. **(C)** The mitochondrial visualization in GD fibroblasts with AMB and EGT treatment for five days. Scale bar represents 100 μm. **(D)** Quantification of fluorescent intensities of mitochondria in GD cells. The signal intensity in untreated cells was set at 100%. Values are expressed as average ±STDEV. * $p<0.05$ compared with an untreated group. **(E)** The mitochondrial visualization in live GD3 fibroblasts. Representative images were assessed in regards to the degree of mitochondrial branching.

https://doi.org/10.1371/journal.pone.0247211.g006

A

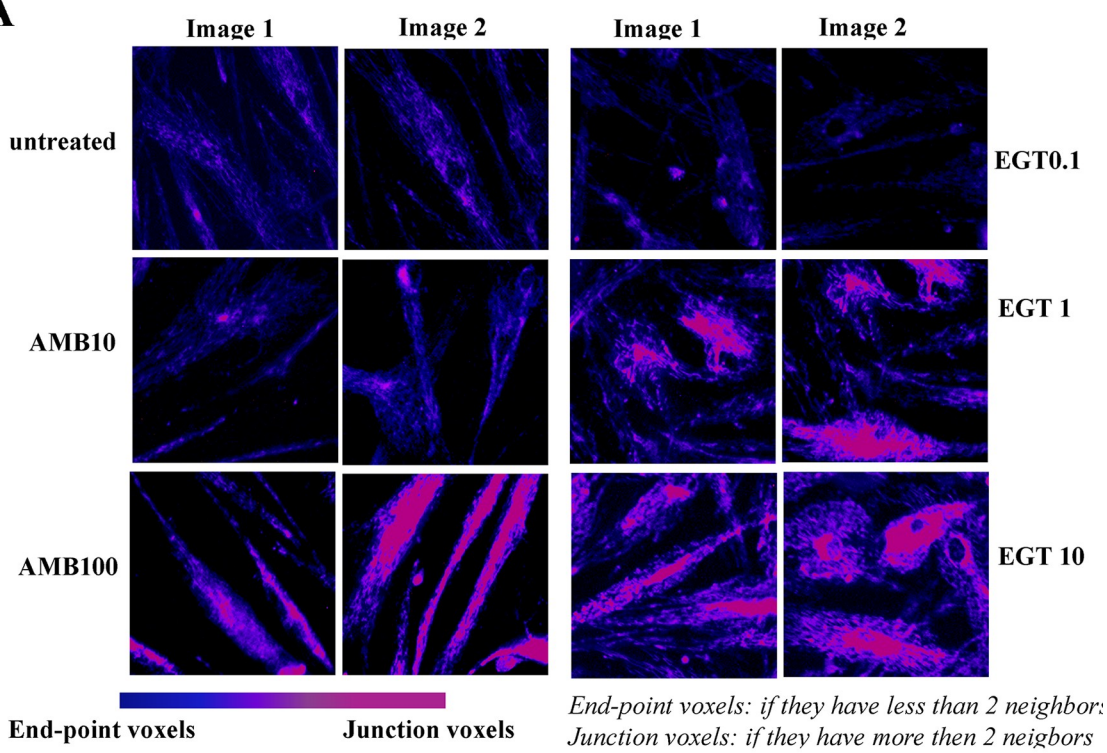

B

	Average			
Treatment	Junction voxels	P value	End point voxels	P value
Untreated	172 ± 3.3		0.20 ± 0.01	
AMB 10 μM	120.2 ± 10.9	0.0036	0.43 ± 0.08	0.008
AMB 100 μM	236 ± 15.3	0.0022	0.50 ± 0.05	0.0004
EGT 0.1 μM	118 ± 8.5	0.0005	0.46 ± 0.03	0.0002
EGT 1 μM	278 ± 42.8	0.0130	0.43 ± 0.04	0.0009
EGT 10 μM	62383 ± 4819.4	0.0001	0.50 ± 0.2	0.05

Fig 7. The skeleton algorithm identifies mitochondrial density in sample images from cells. (A) Post-processed images of living mitochondria stained with MitoTracker. Control fibroblasts were treated with AMB and EGT for five days. Two-tone color (blue turn to pink) represents the intensity of density. **(B)** Results of the corresponding mitochondrial assessment using skeleton 2D/3D analysis.

https://doi.org/10.1371/journal.pone.0247211.g007

AMB and EGT treatments, there were more cells with an increased ΔΨ (S6A Fig) and a shift to P2 (56.2% untreated versus 64.7% and 61.2% AMB and EGT respectively) or P4 population (6.4% untreated versus 19.7% and 11.5% AMB and EGT respectively) (S6B Fig). 100 μM of AMB treatment increased green and red fluorescence intensity signal, especially in PBMC, indicating the presence of both cytoplasmic JC-1 monomer and mitochondrial J-aggregates in cells (Fig 8 and S6 Fig). The higher the ΔΨm, the higher the energy capacity of the inner mitochondrial membrane, thus increasing ATP synthesis. However, the change in inner membrane ion leaks can compromise ΔΨm and potentially be harmful to the mitochondria [31, 32].

Discussion

Currently, there is no available therapy that can prevent, slow, or halt the neurodegenerative process in GD. However, small molecules that can cross the intact BBB and enhance GCase

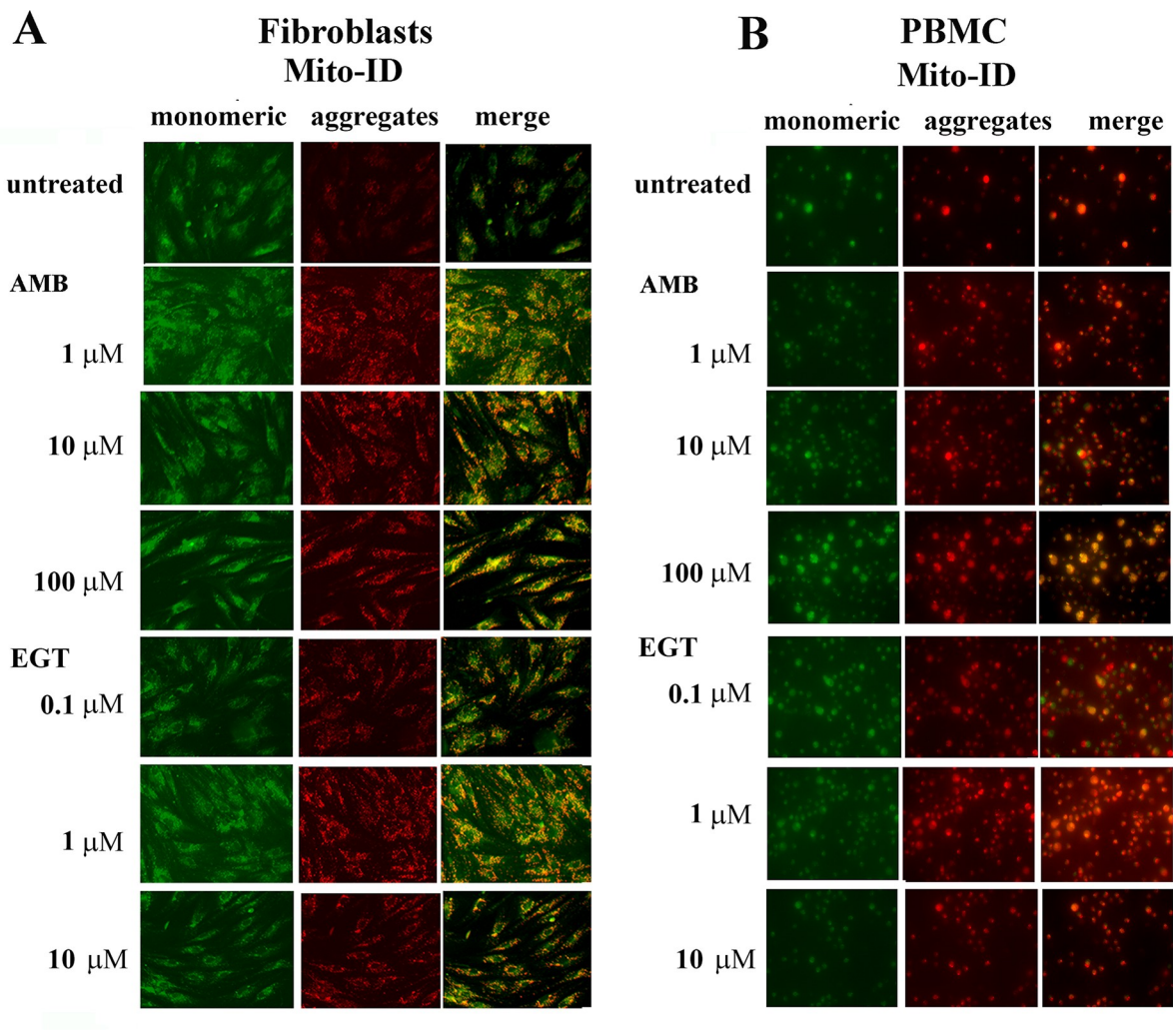

Fig 8. The effects of EGT and AMB on mitochondrial membrane potential in GD. Fibroblasts **(A)** and PBMC **(B)** were treated with increasing concentrations of AMB or EGT for five days, then were stained with Mito-ID Membrane Potential reagent and visualized by fluorescence microscopy. Green represents mitochondria with low membrane potential. Highly polarized mitochondria exhibit red color.

https://doi.org/10.1371/journal.pone.0247211.g008

[33] or inhibit GC accumulation may overcome the limitations of the standard therapeutic approach [34]. Two oral small molecule therapies, SRT and chaperone therapy, are designed to lower the accumulated GC in lysosomes with different mechanisms. In the chaperone therapy strategy, mutated GCase is activated, whereas in the SRT approach GC production is primarily reduced by the inhibition of UGCG synthase. Our results show that the UGCG inhibitor (EGT) and the pharmacologic chaperone (AMB) increase the residual enzymatic activity in primary cell lines from GD2 patients with L444P/L444P;RecΔ55;RecNCiI, and L444P/D409H mutations. However, AMB, but not EGT, increased GCase activity in cells with L444P/L444P;R495P/R495P;A456P mutations. Similar to AMB, EGT did not change the GCase activity in cells with L444P/L444P;D409H;A456P *GBA* mutation. Our data fit previous reports suggesting that the AMB chaperone activity may not simply depend on the type of *GBA* mutation but seems to be individual to a given patient [11, 15, 18]. Other factors that can be involved in AMB pharmacodynamics may hypothetically surge its efficiency; for example, an increase SapC or LIMP2 levels can also stimulate AMB-induced GCase activity [25].

The cellular pathology in GD starts within the lysosome due to chronic substrate accumulation. GC, as an integral part of glycosphingolipid metabolism, is involved in cell signaling transduction, membrane trafficking, and cytoskeletal processes [35]. Mutant GCase is recognized in cells as a misfolded protein, and instead of being trafficked to the lysosomes, it gets retranslocated to the cytoplasm, where it is degraded via the ubiquitin-proteasome system [18]. Several studies and our results confirm that AMB increases GCase trafficking to the lysosome and rescues the misfolded enzyme from degradation in GD macrophages and fibroblasts [16, 18, 36]. However, little is known about the effects of EGT on the trafficking and activity of GCase, aside from the fact that EGT did not inhibit enzyme activity [37]. Computational molecular docking analysis showed that, unlike AMB, EGT did not exhibit strong binding affinity with the mutant N370S and L444P GCase protein. However, EGT demonstrated some intermolecular hydrogen bonds between protein molecules and chaperone. The biochemical characteristic of EGT makes it less likely that it is a lysosomal GCase activator and thus may act as a secondary effector or a chemical chaperone. Here, we report that EGT increased GCase activity in control, GD2, and GD3 cells. Based on data demonstrating that EGT enhanced GCase transport to the lysosomes, we suggest that improving trafficking and lysosomal pathway in the presence of EGT may explain how GCase may retain some level of functionality by escaping the cell quality control mechanism. This data further supports our hypothesis that the inhibition of the first step of glycosphingolipid synthesis activates cellular trafficking.

Dysfunctional lysosomes impair autophagy by blocking autophagic flux in GD [26, 27, 38] as demonstrated in multiple GD model systems, including GBA mouse models, GBA-/- flies, patient fibroblasts, PBMC, and iPSC- neuronal model with GCase or saposin C deficiency [39–44]. Besides the EGT inhibitory activity and the chaperone activity of AMB, our results reveal that both molecules significantly induce autophagic flux, autophagosome-lysosomal fusion, and increased levels of acidic lysosomes in cells derived from GD2 and GD3 patients. As opposed to *GBA* variant dependent chaperone activity, the activation of autophagy-lysosomal processes in the presence of AMB and EGT is irrespective of *GBA* variants. Several studies have shown that AMB enhances lysosomal function in cellular models of Parkinson's disease and reduces alpha-synuclein build-up, improving neuronal functions [24, 25, 44]. Moreover, AMB triggers lysosomal exocytosis [45]. Similarly, EGT inhibits alpha-synuclein and stimulates autophagy flux in neurons by suppressing AKT-mTOR signaling in neurons [46]. Pharmacological induction of ALP can be a useful mechanism to promote GC clearance and protect cells against secondary toxic effects. The induction of autophagy and reversal of lysosomal dysfunction may reduce neuronal cell death and potentially slow down neurologic disease progression in patients with GD2-3 [47, 48].

AMB and EGT at higher concentrations cause inhibition of cell proliferation in GD2 and GD3 fibroblasts. The highest dose of AMB and EGT yielded a cytotoxic effect on GD cells. Previous *in vitro* studies indicated that 60 μM of AMB has a deleterious effect on wild-type mouse embryonic primary cortical neurons after 5 days of treatment [44], while the cause of decreased cell viability was not investigated. Other studies demonstrated that AMB did not cause cell death but disturbed mitochondrial membrane permeability [44]. EGT was shown to decrease the frequency of B cell malignancy in mice by the inhibition of UGCG, which also slows the cell proliferation in liver cells [49, 50].

Severe impairment of autophagy in GD2-3 leads to inhibition of mitophagy and mitochondrial metabolism [51], whereas suppression of autophagy and mitophagy in neural cells is associated with progression of neurodegeneration [52]. Many studies have explored mitophagy and energy metabolism in GD2 and GD3 models [26, 53]. However, only a few studies demonstrated that AMB changed the mitochondrial content in mouse neurons [44, 54]. The results

of the cell viability assay indicate that both AMB and EGT induce total ATP production. In GD2-3 fibroblasts, the activation of mitochondria by AMB and EGT demonstrated by an increase in mitochondrial mass and density, and activation of mitochondrial membrane potential indicate that there are similarities in the cellular response to AMB and EGT.

Considering that animal and cell models to study genetic diseases that impact the CNS mostly yield limited results that could not be replicated clinically, primary fibroblasts or PBMC derived from patients are available choices to examine the effects of drugs at the cellular level. Additionally, *in vitro* cell-based assays with cells derived from GD patients may provide data to help assess the efficacy of ambroxol as a chaperone or lysosome stabilizer [15]. Fibroblasts have been traditionally used to study cellular pathology of lysosomal storage disorders, neurodegenerative diseases mitochondrial dysfunction, and autophagy/lysosomal activation [55–57]. However, the main drawback of the primary fibroblast and PBMC is that they are different than neuronal cells in terms of proliferation rate and different sensitivities to pharmacological treatments.

Conclusion

This study provides evidence towards enhancing our understanding of the cellular mechanisms of GCase chaperone and GC substrate reduction therapies in GD. While substrate synthesis inhibition and pharmacologic chaperone therapies have different modes of action, their downstream effects both enhance GCase activity and improve lysosomal and mitochondrial functions. Our data further supports the proposition that AMB can be used as chaperone therapy for the neuronopathic forms of GD in patients with a positive response to AMB. Thus, the primary cells derived from patients can be considered for evaluating GCase activity and clinical validation of AMB and EGT.

Supporting information

S1 Fig. Assessment of AMB and EGT activity in PBMC and macrophages. A. PBMC derived from healthy controls (n = 5) and GD3 patients with genotypes L444P/L444P and L444P/R502C were cultured for 5 days in the presence of 100μM AMB and 10 μM EGT. Relative GCase activity was estimated as a fold change towards untreated control. Each bar represents the average +/- STDEV. * $p<0.05$ compared with an untreated group. **B.** PBMC and macrophages derived from three GD3 patients with the genotype L444P/L444P, as indicated in the figure, were treated for 5 days in the presence of AMB and EGT. Relative GCase activity was estimated as fold change towards untreated control. Each bar represents the average +/- STDEV. * $p<0.05$ compared with an untreated group.
(TIF)

S2 Fig. EGT and AMB increase autophagosome-lysosome fusion in PBMC. Autophagosome (green, DALGreen) and lysosome (red, LysoTracker) colocalization analysis in PBMC derived from healthy control and GD3 patients (P12, P13, and P14) with the genotype L444P/L444P.
(TIF)

S3 Fig. Cell viability and metabolic status in individual GD2 and GD3 fibroblast cell lines. A. P5 fibroblasts from patients with L444P/L444P were treated with 1, 10, 100 μM of AMB and 0.1, 1,10 μM of EGT for 5 days. The CCK-8 cell viability assay, ATP content, and ATP/CCK-8 (cell viability) ratio were analyzed. The cell counting assay, CCK-8, and ATP results were normalized in relationship to the untreated cells. **B.** P6 fibroblasts with L444P/L444P;RecΔ55;Rec NCiI were treated with 1, 10, 100 μM of AMB and 0.1, 1,10 μM of EGT for 5 days. The CCK-8

cell viability assay, ATP content, and ATP/CCK-8 (cell viability) ratio were analyzed. The cell counting assay, CCK-8, and ATP results were normalized to the untreated cells. **C.** P7 fibroblasts derived from a patient with L444P/L444P;R495P/R495P;A456P mutation were treated with 1, 10, 100 μM of AMB and 0.1, 1,10 μM of EGT for 5 days. The CCK-8 cell viability assay, ATP content, and ATP/CCK-8 ratio were analyzed. The cell counting assay, CCK-8, and ATP results were normalized to the untreated cells. **D.** P9 fibroblasts with L444P/D409H were treated with 1, 10, 100 μM of AMB and 0.1, 1,10 μM of EGT for 5 days. The CCK-8 assay, ATP content, and ATP/CCK-8 ratio were analyzed. The results were normalized to the untreated cells. Values are expressed as average ± SEM. * $p<0.05$ compared with an untreated group.
(TIF)

S4 Fig. Time course of cell viability in individual GD2 and GD3 fibroblast cell lines. A. P5 fibroblasts derived from patient(s) with the *GBA* genotype L444P/L444P were treated with AMB and EGT for 24, 48, 72 h, and 5 days. The CCK-8 was analyzed, and results were normalized to the untreated cells. **B.** P6 fibroblasts were treated with AMB and EGT for 24, 48, 72 h, and 5 days. The CCK-8 assay was measured, and results were normalized to the untreated cells. **C.** P7 fibroblasts were treated with AMB and EGT for 24, 48, 72 h, and 5 days. The CCK-8 assay was measured, and results were normalized to the untreated cells. Values are expressed as average ±SEM. * $p<0.05$ compared with an untreated group.
(TIF)

S5 Fig. Lactate dehydrogenase (LDH) assay. Control and GD3 fibroblasts with L444P/L444P were treated with AMB EGT for 5 days. The LDH assay was analyzed, and results were normalized to the untreated cells. The data represents +/- SEM.
(TIF)

S6 Fig. Effect of the AMB and EGT treatments on mitochondrial membrane potential (Δψ). PBMC derived from GD3 patient were treated with AMB and EGT for 5 days. The JC-1 assay was measured Δψ using Flow cytometry. **A.** Histogram **of** JC-1 red (left) and green (right) fluorescence intensity of mitochondrial polarization. AMB and EGT induce JC-1 aggregations, as is shown by a shift towards increasing red fluorescent signal. **B**. Scatterplot shows the identification of cells with polarized (light green) and depolarized (red) mitochondria in GD3 samples. Double-stained cells are present in areas P1, P2, and P4. Cells with preferential green staining are found in area P3.
(TIF)

S7 Fig. Original western blots from Figs 3D, 3E, 4D, 4E and 4F.
(TIF)

Author Contributions

Conceptualization: Margarita M. Ivanova, Ozlem Goker-Alpan.

Data curation: Margarita M. Ivanova, Ozlem Goker-Alpan.

Formal analysis: Margarita M. Ivanova, Julia Dao, Ozlem Goker-Alpan.

Funding acquisition: Ozlem Goker-Alpan.

Investigation: Margarita M. Ivanova, Julia Dao, Neil Kasaci, Benjamin Adewale, Shaista Nazari, Lauren Noll, Jacqueline Fikry, Armaghan Hafez Sanati.

Methodology: Margarita M. Ivanova, Ozlem Goker-Alpan.

Project administration: Margarita M. Ivanova, Ozlem Goker-Alpan.

Resources: Lauren Noll, Jacqueline Fikry, Ozlem Goker-Alpan.

Supervision: Margarita M. Ivanova, Ozlem Goker-Alpan.

Validation: Margarita M. Ivanova.

Visualization: Margarita M. Ivanova, Julia Dao, Neil Kasaci, Benjamin Adewale.

Writing – original draft: Margarita M. Ivanova, Julia Dao.

Writing – review & editing: Margarita M. Ivanova, Ozlem Goker-Alpan.

References

1. Butters TD (2007) Gaucher disease. Curr Opin Chem Biol 11: 412–418. https://doi.org/10.1016/j.cbpa.2007.05.035 PMID: 17644022
2. Stirnemann J, Belmatoug N, Camou F, Serratrice C, Froissart R, et al. (2017) A Review of Gaucher Disease Pathophysiology, Clinical Presentation and Treatments. Int J Mol Sci 18. https://doi.org/10.3390/ijms18020441 PMID: 28218669
3. Bennett LL, Fellner C (2018) Pharmacotherapy of Gaucher Disease: Current and Future Options. P T 43: 274–309. PMID: 29719368
4. Schwartz IVD, Goker-Alpan O, Kishnani PS, Zimran A, Renault L, et al. (2018) Characteristics of 26 patients with type 3 Gaucher disease: A descriptive analysis from the Gaucher Outcome Survey. Mol Genet Metab Rep 14: 73–79. https://doi.org/10.1016/j.ymgmr.2017.10.011 PMID: 29326879
5. Zimran A, Elstein D (2014) Management of Gaucher disease: enzyme replacement therapy. Pediatr Endocrinol Rev 12 Suppl 1: 82–87. PMID: 25345089
6. Parenti G (2009) Treating lysosomal storage diseases with pharmacological chaperones: from concept to clinics. EMBO Mol Med 1: 268–279. https://doi.org/10.1002/emmm.200900036 PMID: 20049730
7. Peterschmitt MJ, Freisens S, Underhill LH, Foster MC, Lewis G, et al. (2019) Long-term adverse event profile from four completed trials of oral eliglustat in adults with Gaucher disease type 1. Orphanet J Rare Dis 14: 128. https://doi.org/10.1186/s13023-019-1085-6 PMID: 31174576
8. Shayman JA (2010) ELIGLUSTAT TARTRATE: Glucosylceramide Synthase Inhibitor Treatment of Type 1 Gaucher Disease. Drugs Future 35: 613–620. PMID: 22563139
9. Cox TM, Drelichman G, Cravo R, Balwani M, Burrow TA, et al. (2017) Eliglustat maintains long-term clinical stability in patients with Gaucher disease type 1 stabilized on enzyme therapy. Blood 129: 2375–2383. https://doi.org/10.1182/blood-2016-12-758409 PMID: 28167660
10. Sardi SP, Viel C, Clarke J, Treleaven CM, Richards AM, et al. (2017) Glucosylceramide synthase inhibition alleviates aberrations in synucleinopathy models. Proc Natl Acad Sci U S A 114: 2699–2704. https://doi.org/10.1073/pnas.1616152114 PMID: 28223512
11. Maegawa GH, Tropak MB, Buttner JD, Rigat BA, Fuller M, et al. (2009) Identification and characterization of ambroxol as an enzyme enhancement agent for Gaucher disease. J Biol Chem 284: 23502–23516. https://doi.org/10.1074/jbc.M109.012393 PMID: 19578116
12. Zimran A, Altarescu G, Elstein D (2013) Pilot study using ambroxol as a pharmacological chaperone in type 1 Gaucher disease. Blood Cells Mol Dis 50: 134–137. https://doi.org/10.1016/j.bcmd.2012.09.006 PMID: 23085429
13. Narita A, Shirai K, Itamura S, Matsuda A, Ishihara A, et al. (2016) Ambroxol chaperone therapy for neuronopathic Gaucher disease: A pilot study. Ann Clin Transl Neurol 3: 200–215. https://doi.org/10.1002/acn3.292 PMID: 27042680
14. Charkhand B, Scantlebury MH, Narita A, Zimran A, Al-Hertani W (2019) Effect of Ambroxol chaperone therapy on Glucosylsphingosine (Lyso-Gb1) levels in two Canadian patients with type 3 Gaucher disease. Mol Genet Metab Rep 20: 100476. https://doi.org/10.1016/j.ymgmr.2019.100476 PMID: 31467847
15. Ivanova MM, Changsila E, Turgut A, Goker-Alpan O (2018) Individualized screening for chaperone activity in Gaucher disease using multiple patient derived primary cell lines. Am J Transl Res 10: 3750–3761. PMID: 30662625
16. Kopytova AE, Rychkov GN, Nikolaev MA, Baydakova GV, Cheblokov AA, et al. (2021) Ambroxol increases glucocerebrosidase (GCase) activity and restores GCase translocation in primary patient-derived macrophages in Gaucher disease and Parkinsonism. Parkinsonism Relat Disord 84: 112–121. https://doi.org/10.1016/j.parkreldis.2021.02.003 PMID: 33609962

17. Luan Z, Li L, Higaki K, Nanba E, Suzuki Y, et al. (2013) The chaperone activity and toxicity of ambroxol on Gaucher cells and normal mice. Brain Dev 35: 317–322. https://doi.org/10.1016/j.braindev.2012.05.008 PMID: 22682976

18. Bendikov-Bar I, Maor G, Filocamo M, Horowitz M (2013) Ambroxol as a pharmacological chaperone for mutant glucocerebrosidase. Blood Cells Mol Dis 50: 141–145. https://doi.org/10.1016/j.bcmd.2012.10.007 PMID: 23158495

19. Halter D, Neumann S, van Dijk SM, Wolthoorn J, de Maziere AM, et al. (2007) Pre- and post-Golgi translocation of glucosylceramide in glycosphingolipid synthesis. J Cell Biol 179: 101–115. https://doi.org/10.1083/jcb.200704091 PMID: 17923531

20. Tamargo RJ, Velayati A, Goldin E, Sidransky E (2012) The role of saposin C in Gaucher disease. Mol Genet Metab 106: 257–263. https://doi.org/10.1016/j.ymgme.2012.04.024 PMID: 22652185

21. Urban DJ, Zheng W, Goker-Alpan O, Jadhav A, Lamarca ME, et al. (2008) Optimization and validation of two miniaturized glucocerebrosidase enzyme assays for high throughput screening. Comb Chem High Throughput Screen 11: 817–824. https://doi.org/10.2174/138620708786734244 PMID: 19075603

22. Zheng W, Padia J, Urban DJ, Jadhav A, Goker-Alpan O, et al. (2007) Three classes of glucocerebrosidase inhibitors identified by quantitative high-throughput screening are chaperone leads for Gaucher disease. Proc Natl Acad Sci U S A 104: 13192–13197. https://doi.org/10.1073/pnas.0705637104 PMID: 17670938

23. Nikolaisen J, Nilsson LI, Pettersen IK, Willems PH, Lorens JB, et al. (2014) Automated quantification and integrative analysis of 2D and 3D mitochondrial shape and network properties. PLoS One 9: e101365. https://doi.org/10.1371/journal.pone.0101365 PMID: 24988307

24. McNeill A, Magalhaes J, Shen C, Chau KY, Hughes D, et al. (2014) Ambroxol improves lysosomal biochemistry in glucocerebrosidase mutation-linked Parkinson disease cells. Brain 137: 1481–1495. https://doi.org/10.1093/brain/awu020 PMID: 24574503

25. Ambrosi G, Ghezzi C, Zangaglia R, Levandis G, Pacchetti C, et al. (2015) Ambroxol-induced rescue of defective glucocerebrosidase is associated with increased LIMP-2 and saposin C levels in GBA1 mutant Parkinson's disease cells. Neurobiol Dis 82: 235–242. https://doi.org/10.1016/j.nbd.2015.06.008 PMID: 26094596

26. Ivanova MM, Changsila E, Iaonou C, Goker-Alpan O (2019) Impaired autophagic and mitochondrial functions are partially restored by ERT in Gaucher and Fabry diseases. PLoS One 14: e0210617. https://doi.org/10.1371/journal.pone.0210617 PMID: 30633777

27. Kinghorn KJ, Asghari AM, Castillo-Quan JI (2017) The emerging role of autophagic-lysosomal dysfunction in Gaucher disease and Parkinson's disease. Neural Regen Res 12: 380–384. https://doi.org/10.4103/1673-5374.202934 PMID: 28469644

28. Iwashita H, Sakurai HT, Nagahora N, Ishiyama M, Shioji K, et al. (2018) Small fluorescent molecules for monitoring autophagic flux. FEBS Lett 592: 559–567. https://doi.org/10.1002/1873-3468.12979 PMID: 29355929

29. Ouellet M, Guillebaud G, Gervais V, Lupien St-Pierre D, Germain M (2017) A novel algorithm identifies stress-induced alterations in mitochondrial connectivity and inner membrane structure from confocal images. PLoS Comput Biol 13: e1005612. https://doi.org/10.1371/journal.pcbi.1005612 PMID: 28640814

30. Leonard AP, Cameron RB, Speiser JL, Wolf BJ, Peterson YK, et al. (2015) Quantitative analysis of mitochondrial morphology and membrane potential in living cells using high-content imaging, machine learning, and morphological binning. Biochim Biophys Acta 1853: 348–360. https://doi.org/10.1016/j.bbamcr.2014.11.002 PMID: 25447550

31. Zorova LD, Popkov VA, Plotnikov EY, Silachev DN, Pevzner IB, et al. (2018) Mitochondrial membrane potential. Anal Biochem 552: 50–59. https://doi.org/10.1016/j.ab.2017.07.009 PMID: 28711444

32. Skulachev VP (1996) Role of uncoupled and non-coupled oxidations in maintenance of safely low levels of oxygen and its one-electron reductants. Q Rev Biophys 29: 169–202. https://doi.org/10.1017/s0033583500005795 PMID: 8870073

33. Migdalska-Richards A, Ko WKD, Li Q, Bezard E, Schapira AHV (2017) Oral ambroxol increases brain glucocerebrosidase activity in a nonhuman primate. Synapse 71.

34. Han TU, Sam R, Sidransky E (2020) Small Molecule Chaperones for the Treatment of Gaucher Disease and GBA1-Associated Parkinson Disease. Front Cell Dev Biol 8: 271. https://doi.org/10.3389/fcell.2020.00271 PMID: 32509770

35. van Meer G, Wolthoorn J, Degroote S (2003) The fate and function of glycosphingolipid glucosylceramide. Philos Trans R Soc Lond B Biol Sci 358: 869–873. https://doi.org/10.1098/rstb.2003.1266 PMID: 12803919

36. Panicker LM, Miller D, Awad O, Bose V, Lun Y, et al. (2014) Gaucher iPSC-derived macrophages produce elevated levels of inflammatory mediators and serve as a new platform for therapeutic development. Stem Cells 32: 2338–2349. https://doi.org/10.1002/stem.1732 PMID: 24801745

37. McEachern KA, Fung J, Komarnitsky S, Siegel CS, Chuang WL, et al. (2007) A specific and potent inhibitor of glucosylceramide synthase for substrate inhibition therapy of Gaucher disease. Mol Genet Metab 91: 259–267. https://doi.org/10.1016/j.ymgme.2007.04.001 PMID: 17509920

38. Kinghorn KJ, Gronke S, Castillo-Quan JI, Woodling NS, Li L, et al. (2016) A Drosophila Model of Neuronopathic Gaucher Disease Demonstrates Lysosomal-Autophagic Defects and Altered mTOR Signalling and Is Functionally Rescued by Rapamycin. J Neurosci 36: 11654–11670. https://doi.org/10.1523/JNEUROSCI.4527-15.2016 PMID: 27852774

39. Sun Y, Liou B, Ran H, Skelton MR, Williams MT, et al. (2010) Neuronopathic Gaucher disease in the mouse: viable combined selective saposin C deficiency and mutant glucocerebrosidase (V394L) mice with glucosylsphingosine and glucosylceramide accumulation and progressive neurological deficits. Hum Mol Genet 19: 1088–1097. https://doi.org/10.1093/hmg/ddp580 PMID: 20047948

40. Vaccaro AM, Motta M, Tatti M, Scarpa S, Masuelli L, et al. (2010) Saposin C mutations in Gaucher disease patients resulting in lysosomal lipid accumulation, saposin C deficiency, but normal prosaposin processing and sorting. Hum Mol Genet 19: 2987–2997. https://doi.org/10.1093/hmg/ddq204 PMID: 20484222

41. Osellame LD, Rahim AA, Hargreaves IP, Gegg ME, Richard-Londt A, et al. (2013) Mitochondria and quality control defects in a mouse model of Gaucher disease—links to Parkinson's disease. Cell Metab 17: 941–953. https://doi.org/10.1016/j.cmet.2013.04.014 PMID: 23707074

42. Farfel-Becker T, Vitner EB, Kelly SL, Bame JR, Duan J, et al. (2014) Neuronal accumulation of glucosylceramide in a mouse model of neuronopathic Gaucher disease leads to neurodegeneration. Hum Mol Genet 23: 843–854. https://doi.org/10.1093/hmg/ddt468 PMID: 24064337

43. Awad O, Sarkar C, Panicker LM, Miller D, Zeng X, et al. (2015) Altered TFEB-mediated lysosomal biogenesis in Gaucher disease iPSC-derived neuronal cells. Hum Mol Genet 24: 5775–5788. https://doi.org/10.1093/hmg/ddv297 PMID: 26220978

44. Magalhaes J, Gegg ME, Migdalska-Richards A, Schapira AH (2018) Effects of ambroxol on the autophagy-lysosome pathway and mitochondria in primary cortical neurons. Sci Rep 8: 1385. https://doi.org/10.1038/s41598-018-19479-8 PMID: 29362387

45. Fois G, Hobi N, Felder E, Ziegler A, Miklavc P, et al. (2015) A new role for an old drug: Ambroxol triggers lysosomal exocytosis via pH-dependent Ca(2)(+) release from acidic Ca(2)(+) stores. Cell Calcium 58: 628–637. https://doi.org/10.1016/j.ceca.2015.10.002 PMID: 26560688

46. Shen W, Henry AG, Paumier KL, Li L, Mou K, et al. (2014) Inhibition of glucosylceramide synthase stimulates autophagy flux in neurons. J Neurochem 129: 884–894. https://doi.org/10.1111/jnc.12672 PMID: 24494600

47. Son JH, Shim JH, Kim KH, Ha JY, Han JY (2012) Neuronal autophagy and neurodegenerative diseases. Exp Mol Med 44: 89–98. https://doi.org/10.3858/emm.2012.44.2.031 PMID: 22257884

48. Palhegyi AM, Seranova E, Dimova S, Hoque S, Sarkar S (2019) Biomedical Implications of Autophagy in Macromolecule Storage Disorders. Front Cell Dev Biol 7: 179. https://doi.org/10.3389/fcell.2019.00179 PMID: 31555645

49. Li JF, Zheng SJ, Wang LL, Liu S, Ren F, et al. (2017) Glucosylceramide synthase regulates the proliferation and apoptosis of liver cells in vitro by Bcl2/Bax pathway. Mol Med Rep 16: 7355–7360. https://doi.org/10.3892/mmr.2017.7580 PMID: 28944894

50. Pavlova EV, Archer J, Wang S, Dekker N, Aerts JM, et al. (2015) Inhibition of UDP-glucosylceramide synthase in mice prevents Gaucher disease-associated B-cell malignancy. J Pathol 235: 113–124. https://doi.org/10.1002/path.4452 PMID: 25256118

51. Ivanova M (2020) Altered Sphingolipids Metabolism Damaged Mitochondrial Functions: Lessons Learned From Gaucher and Fabry Diseases. J Clin Med 9. https://doi.org/10.3390/jcm9041116 PMID: 32295103

52. Martinez-Vicente M (2017) Neuronal Mitophagy in Neurodegenerative Diseases. Front Mol Neurosci 10: 64. https://doi.org/10.3389/fnmol.2017.00064 PMID: 28337125

53. de la Mata M, Cotan D, Villanueva-Paz M, de Lavera I, Alvarez-Cordoba M, et al. (2016) Mitochondrial Dysfunction in Lysosomal Storage Disorders. Diseases 4. https://doi.org/10.3390/diseases4040031 PMID: 28933411

54. Magalhaes J, Gegg ME, Migdalska-Richards A, Doherty MK, Whitfield PD, et al. (2016) Autophagic lysosome reformation dysfunction in glucocerebrosidase deficient cells: relevance to Parkinson disease. Hum Mol Genet 25: 3432–3445. https://doi.org/10.1093/hmg/ddw185 PMID: 27378698

55. Mak SK, Tewari D, Tetrud JW, Langston JW, Schule B (2011) Mitochondrial dysfunction in skin fibroblasts from a Parkinson's disease patient with an alpha-synuclein triplication. J Parkinsons Dis 1: 175–183. https://doi.org/10.3233/JPD-2011-11025 PMID: 23934919

56. Perez MJ, Ponce DP, Osorio-Fuentealba C, Behrens MI, Quintanilla RA (2017) Mitochondrial Bioenergetics Is Altered in Fibroblasts from Patients with Sporadic Alzheimer's Disease. Front Neurosci 11: 553. https://doi.org/10.3389/fnins.2017.00553 PMID: 29056898

57. Auburger G, Klinkenberg M, Drost J, Marcus K, Morales-Gordo B, et al. (2012) Primary skin fibroblasts as a model of Parkinson's disease. Mol Neurobiol 46: 20–27. https://doi.org/10.1007/s12035-012-8245-1 PMID: 22350618